

ISOTROPY IN THE CONTEXTUAL EMBEDDING SPACE: CLUSTERS AND MANIFOLDS

Anonymous authors

Paper under double-blind review

ABSTRACT

The geometric properties of contextual embedding spaces for deep language models such as BERT and ERNIE, have attracted considerable attention in recent years. Investigations on the contextual embeddings demonstrate a strong anisotropic space such that most of the vectors fall within a narrow cone, leading to high cosine similarities. It is surprising that these LMs are as successful as they are, given that most of their embedding vectors are as similar to one another as they are. In this paper, we argue that the isotropy indeed exists in the space, from a different but more constructive perspective. We identify isolated clusters and low dimensional manifolds in the contextual embedding space, and introduce tools to both qualitatively and quantitatively analyze them. We hope the study in this paper could provide insights towards a better understanding of the deep language models.

1 INTRODUCTION

Consider the polysemous English word “bank”. There are two common senses: 1. the money sense, a place that people save or borrow money; 2. the river sense, a slope of earth that prevents the flooding. In modern usage, the two senses are very different from one another, though interestingly, both senses share similar etymologies (and both can be traced back to the same word in Proto-Germanic). In the **static embedding**, multiple instances of the same word (“bank” in above example) will be represented using the same vector. On the contrary, the **contextual embedding** assigns different vectors to different instances of the same word, depending on the context. Historically, static embedding models like Word2vec (Mikolov et al., 2013b) and GloVe (Pennington et al., 2014), predated contextual embedding models such as ELMo (Peters et al., 2018), GPT (Radford et al., 2018), BERT (Devlin et al., 2018) and ERNIE (Sun et al., 2019). Much of the literature on language modeling has moved to contextual embeddings recently, largely because of their superior performance on almost all the downstream tasks.

1.1 RELATED WORK

The static embeddings are often found to be easier to interpret. For example, the Word2Vec and GloVe papers discuss adding and subtracting vectors, such as: $\text{vec}(\text{king}) - \text{vec}(\text{man}) + \text{vec}(\text{women}) = \text{vec}(\text{queen})$. Inspired by this relationship, researchers started to explore geometric properties of static embedding spaces. For example, Mu & Viswanath (2018) proposed a very counter-intuitive method that removes the top principle components (the dominating directions in the transformed embedding space), which surprisingly, improved the representation, as validated on a variety of tasks. Rather than completely discarding the principle components, Liu et al. (2019) proposed to use a technique called Conceptor Negation, to softly suppress transformed dimensions with larger variances. Both approaches, simply removing certain principle components as well as Conceptor Negation, produce significant improvements over vanilla embeddings obtained by static language models.

Unfortunately, the strong illustrative representation like the king-queen example above, is no longer obvious in a general contextual embedding space. Arguing that syntax structure indeed exists in the contextual embeddings, Hewitt & Manning (2019) proposed a structural probe to identify the syntax trees buried in the space, and found the evidence of implicit syntax tree in BERT and ELMo. The advantage of contextual embedding over the static counterpart, mainly come from its capability to assign different vectors to the same word, depending on the word sense in the context. Researchers in (Reif et al., 2019) found such a geometric representation of word senses in the BERT model. These papers reveal the existence of linguistic features embedded implicitly in the contextual vector spaces.

The geometric properties of contextual embedding space are also investigated and compared with the static embedding space. In (Ethayarajh, 2019), the authors characterize how vectors are distributed in the contextual space. They found that most vectors occupy in a relatively narrow cone in the

space. Pairs of vectors within this cone have large cosines. This phenomenon can be found in most state-of-the-art contextual embedding models. In (Gao et al., 2019), the authors named this phenomenon "representation degeneration" problem and attempted to mitigate the problem by introducing a regularization term that minimizes cosine similarities between vectors. In a very recent work, Demeter et al. (2020) suggest there is a structure weakness in the space that leads to bias when using soft-max, as is common with deep LMs.

1.2 MOTIVATION AND CONTRIBUTIONS

There is an apparent contradiction. It is extremely counter-intuitive that the contextual embedding models perform remarkably well on many tasks (state-of-the-art performance) even though their embeddings bring all the vectors close together, making it hard to distinguish one vector from another. Moreover, on one hand, it is widely believed (e.g. (Reif et al., 2019)) that contextual embeddings encode the relevant linguistic information, but on the other hand, it is also widely believed that the contextual space is so weird/anisotropic that representations become degenerated. These apparent contradictions motivate us to find a reasonable understanding that bridges this gap.

This paper is similar in spirit to (Mu & Viswanath, 2018), but different in three aspects. First, we generalize their work on older static embeddings to more modern contextual embeddings. Second, we introduce clustering methods to isolate the space, whereas they used PCA to remove dominant dimensions (that tend to dominate the variance). Finally, we identify low dimensional manifolds in the space, and introduce an alternative approach (LID) to characterize local subspaces.

Key Contributions: This paper takes a deeper look into contextual embedding spaces of popular pre-trained models. It identifies the following facts that were misunderstood or not known before: 1) We find isotropy in contextual embedding space, in contrast to previous reports of anisotropy (caused by misleading isolated clusters). We introduce clustering and center shifting to reveal the isotropicity, and show more consistent layer-wise behavior across models. 2) We find a low-dimensional manifold in GPT/GPT2 embeddings, but not in BERT/DistilBERT embeddings. The manifold is related to word frequency, suggesting a difference in how models evolve as they see more data. We use approximate Local Intrinsic Dimension (LID) to characterize the manifold, and find contextual embedding models often have small LIDs. The small LIDs can be viewed as the local anisotropy of the space.

2 EXPERIMENTAL SETTINGS

2.1 MODELS AND DATASETS

In this paper, we consider popular pre-trained contextual embedding models, including BERT, DistilBERT (Sanh et al., 2019) (or denoted as D-BERT in the rest of the paper), GPT, GPT2 (Radford et al., 2019) and ELMo. For the BERT and GPT families, we perform our evaluations on the pre-trained uncased base models from Huggingface (<https://huggingface.co/transformers/index.html#>). The pre-trained ELMo model is from AllenNLP (<https://docs.allennlp.org/v1.0.0/>). BERT and D-BERT are **non-causal** models because of their attention mechanism, where tokens can attend to any token in the input, regardless of their relative positions. In contrast, GPT and GPT2 are **causal** models because attention is limited to the tokens previously seen in the input.

Different models achieve contextual embedding in different ways. For instance, BERT adds positional embeddings to the token embeddings, while ELMo performs vector concatenation. Most models start with an initial layer that maps token ids to vectors. This paper is not concerned with that lookup table layer and only focus on the layers after that. The base BERT, GPT and GPT2 models have 12 layers of interest, indexed from 0 to 11, while D-BERT has 6 layers and ELMo has two.

We use Penn Tree Bank (PTB) (Marcus et al., 1993) and Wiki2 (Merity et al., 2016) datasets. The PTB has 0.88 million words and Wiki2 has 2 million. They both provide a good coverage and being the standard datasets for language models. In the rest of the paper, we report on PTB since we see similar results with both datasets. Details on Wiki2 experiments could be found in supplementary.

2.2 NOTATION

For each position in a corpus, we have a **word**. Words are converted into **tokens**, using the appropriate tokenizer for the model. Tokenizers could split some words into subwords, therefore, the number of obtained tokens (denoted as n) could be more than number of words in the corpus. PTB, for example, contains 0.88 million words, but has $n = 1.2$ million tokens, when processed by BERT’s tokenizer. Let V be the **vocabulary**, a set of distinct tokens. For any element in the vocabulary V , we call it

a **type**. For example, BERT has a vocabulary of roughly 30,000 types. We may mix using “word” and “type” for ease of reading. We denote the i -th type in V as t_i . Let $\Phi(t_i) = \{\phi_1(t_i), \phi_2(t_i), \dots\}$ be the set of all embedding instances of t_i (note that different contexts in the corpus yield different embeddings of t_i). By construction, $\sum_t |\Phi(t)| = n$. We define the **inter-type** cosine similarity as

$$S_{\text{inter}} \triangleq \mathbb{E}_{i \neq j} [\cos(\phi(t_i), \phi(t_j))] \quad (1)$$

where $\phi(t_i)$ is one random sample from $\Phi(t_i)$, and the same for $\phi(t_j) \in \Phi(t_j)$. The expectation is taken over all pairs of different types. Similarly, we define the **intra-type** cosine similarity as

$$S_{\text{intra}} \triangleq \mathbb{E}_i [\mathbb{E}_{k \neq l} [\cos(\phi_k(t_i), \phi_l(t_i))]] \quad (2)$$

where the inner expectation is over different embeddings $\phi(t_i)$ for the same type t_i , and the outer expectation is over all types. Note that S_{inter} and S_{intra} take values between -1 and 1 . Note that for i.i.d. Gaussian random samples x, y , the expected cosine similarity $\mathbb{E}[\cos(x, y)] = 0$.

Clearly, the inter-type metric describes the similarity between different types, where the intra-type one measures similarity between same type’s embedding instances. Our definitions of S_{inter} and S_{intra} are similar to the measures used in Ethayarajh (2019), but at the corpus level. Note that some types are more frequent than others, especially under a Zipfian distribution (Piantadosi, 2014), and therefore, the size of $\Phi(t)$ varies dramatically with the frequency of t .

2.3 AN INITIAL LOOK AT ANISOTROPY

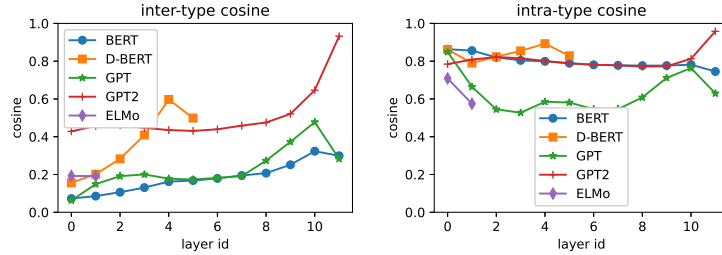


Figure 1: S_{inter} (left) and S_{intra} (right). The S_{inter} increases as layer goes deeper, especially for GPT2’s last layer. The S_{intra} are generally high. This means arbitrary vectors have high cosine similarities.

Figure 1 shows strong anisotropy effects in a number of models. These findings are consistent with Ethayarajh (2019), though we use slightly different metrics. The plots show expected cosine (S_{inter} and S_{intra}) as a function of layer. For efficiency, we approximate S_{intra} by imposing a limit of 1,000 samples for frequent types, t , if $|\Phi(t)| > 1000$. From the figure we can see the following:

- Both S_{inter} and S_{intra} are high ($\gg 0$) across almost all the layers and all the models. In particular, the same as reported in Ethayarajh (2019), GPT2 is relatively more anisotropic.
- S_{inter} tends to increase with layer, in contrast with S_{intra} which in general decreases but with fluctuations. This means that embeddings for different types are moving closer to one another at deeper layers, while embeddings for the same type’s instances are spreading away.
- The last layer is often special. Note that the last layer has smaller cosines than the second last in most cases, with the notable exception of GPT2.

In summary, we observe large cosines (across layers/models), especially for the GPT2 model. When cosines are close to 1, embeddings lie in a subspace defined by a very narrow cone (Ethayarajh, 2019). One might expect embeddings to be more effective if they took advantage of a larger subspace. Are these models missing an opportunity to have the benefits from isotropicity (Mu & Viswanath, 2018)? We answer this question in the following sections.

3 CLUSTERS IN THE EMBEDDING SPACE

3.1 EFFECTIVE DIMENSIONS

There are $m = 768$ embedding dimensions for BERT, D-BERT, GPT and GPT2, and $m = 1024$ dimensions for ELMo. We perform PCA to reduce the number of dimensions from m down to k . For each layer of each model, we start with the data matrix, $M \in \mathcal{R}^{n \times m}$, where n is the number of input tokens ($n = 1.2M$ for PTB dataset), and m is the original number of dimensions. After PCA, we end up with a smaller matrix, $\hat{M} \in \mathcal{R}^{n \times k}$. Let the **explained variance ratio** be:

$r_k = \sum_{i=0}^{k-1} \sigma_i / \sum_{i=0}^{m-1} \sigma_i$, where σ_i is the i -th largest eigen value of M 's covariance matrix. In this way, we define the ϵ -**effective-dimension** to be: $d(\epsilon) \triangleq \arg \min_k r_k \geq \epsilon$. For example, $d(0.8) = 2$ means that 2 dimensions capture 80% of the variance. There is a direct connection between d and isotropicity: the larger d often implies more isotropy, as data spreads in multiple dimensions.

Table 1: The effective dimension $d(0.8)$

Layer	0	1	2	3	4	5	6	7	8	9	10	11
BERT	262	273	271	273	276	283	288	282	282	282	283	270
D-BERT	244	226	232	227	217	175						
GPT	265	141	65	76	173	210	205	217	221	253	269	307
GPT2	114	73	1	1	1	1	1	8	26	66	116	1
ELMo	455	367										

Table 1 reports $d(0.8)$ for different layers and models. It is surprising that GPT2 has so few effective dimensions, especially, $d(0.8) = 1$ for layer 2 to 6. The surprisingly small effective dimensionality is another way of saying that GPT2 vectors fall in a narrow cone, and consequently, their pairwise cosines are large. If all the vectors lie on a 1-D line, all the cosines would be 1, and there would be hardly any model capacity. These observations motivate us to look deeper into the embedding space.

3.2 ISOLATED CLUSTERS

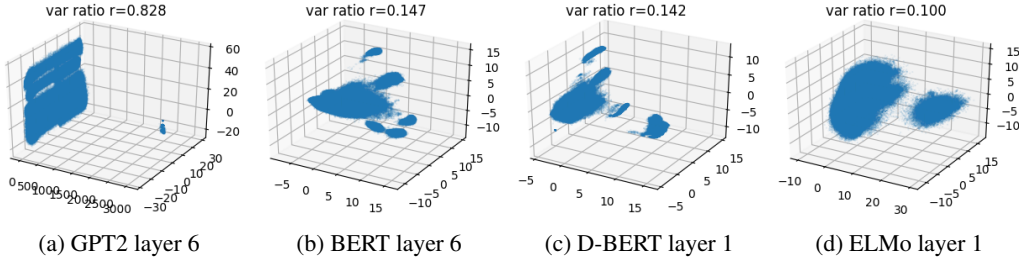


Figure 2: Isolated clusters exist in the embedding spaces for all the models. Here we only show a few representative middle layers for each model. The full visualization can be found in supplementary.

By performing PCA to project the original data into a 3-D view, we can visualize GPT2’s layer 6’s embedding space in Figure 2a. The three axes refer to the first three principle components, which account for 82.8% of the total variance. All the explained variance ratio will be reported throughout the rest of the paper. The axes values are raw coordinates after PCA. In Figure 2a, there are two disconnected islands that are far away from each other. Note that the first dimension coordinate values spans from 0 to 3000, significantly wider than the other 2 dimensions. In fact this first principle dimension dominates the total variance. The left island is bigger than the one on the right. The fact that the two islands are so well separated by the first principle component suggests that classifying points by island membership accounts for much of the variance. This two-island property is exhibited in layers 2 through 10 for GPT2. The two islands merge into a single large cluster in the last layer.

We observe similar clustering behavior for all the models across all the layers, though the separations are less distinct, as illustrated in other panels of Figure 2. This is also consistent with Table 1, the less separation, the higher $d(\epsilon)$ values. For GPT2, we had hoped to find that some types are associated with one cluster and other types are associated with the other cluster, but that is not verified in our experiments. Please refer to the supplementary for visualizations of all layers in all the models.

3.3 CLUSTERING

Previous literature estimated the space isotropicity on pairs of arbitrary tokens, which could reside in two disconnected clusters. But given that the variance is dominated by distances between clusters, such estimation would be biased by the inter-cluster distances. It is more meaningful to consider a per-cluster investigation rather than a global estimate.

We start by performing clustering on the embedding space. There are many methods for clustering. We chose K-Means (<https://scikit-learn.org/stable/modules/classes.html#>), because it is reasonably fast for large inputs ($n = 1.2$ million vectors) in high ($m \geq 768$) dimensions. DBSCAN algorithm (Ester et al., 1996) could be an alternative as it is density based, but only works on small dataset. We use the Silhouette method (Rousseeuw, 1987) to determine the number of clusters, $|C|$. After running K-means, each point p (one of the n vectors in M) is assigned to one of C clusters. For a data point

p assigned to the cluster $c \in C$, calculate the following:

$$a_p = \frac{1}{|c| - 1} \sum_{q \in c, p \neq q} \text{dist}(p, q) ; \quad b_p = \min_{\tilde{c} \neq c} \sum_{q \in \tilde{c}} \text{dist}(p, q) ; \quad s_p = \begin{cases} \frac{b_p - a_p}{\max(a_p, b_p)}, & \text{if } |c| > 1 \\ 0, & \text{otherwise} \end{cases}$$

where a_p is the mean distance between p and other points in the same cluster; b_p is the minimum (min over \tilde{c}) mean distance between p to points of another cluster \tilde{c} ; and s_p is the Silhouette score for point $p \in c$. The s_p takes value $\in [-1, 1]$. The higher s_p , the better assignment of p to its cluster. Better choices of $|C|$ would lead to better values of s_p (and better clustering). We define the **Maximum-Mean-Silhouette** (MMS) score for the embedding space as: $\text{MMS} \triangleq \max_{\text{different } |C|} \mathbb{E}_p[s_p]$, where the maximum is over different $|C|$ values for K-Means. Since it is not feasible to evaluating all choices of $|C| \in [1, n]$, we consider $|C| \in [1, 15]$. The expectation $\mathbb{E}_p[s_p]$ (the mean Silhouette score), is estimated from 20,000 sample vectors in M . We select the best $|C|$ that yields MMS.

The MMS values provide a systematic way to describe how the clusters are distributed in the space. If the clusters are very distinct and splitted, this yields a higher MMS. On the other hand, if clusters are overlapping, blurring together, the MMS score will be low. Note that if $\text{MMS} < 0.1$, we set $|C|$ to be 1, as the Silhouette score does not show significant evidence of more clusters.

Table 2: Number of clusters $|C|$

Layer	BERT	D-BERT	GPT	GPT2	ELMo
0	6	7	1	2	2
1	6	10	2	2	2
2	4	15	2	2	
3	4	14	2	2	
4	3	10	2	2	
5	14	2	2	2	
6	6		2	2	
7	2		2	2	
8	2		2	2	
9	11		1	2	
10	2		1	2	
11	9		1	2	

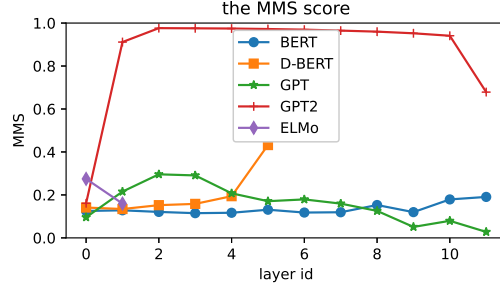


Figure 3: The MMS for all the models. GPT2 has significantly higher MMS scores than other models from layer 1 to layer 11. This means the cluster effects are more severe in GPT2.

Table 2 makes it clear that clustering plays an important role in most layers of most models. Some models (BERT and D-BERT) have more clusters, and some have fewer (GPT, GPT2, ELMo). This dichotomy of models is also reflected in Figure 2.

Maximum-Mean-Silhouette scores are shown in Figure 3. There are significantly higher MMS values for GPT2, starting from the 2nd layer. Recall in Figure 2a, we showed that two far-away islands exist in the space and their distance dominates the variance. In Figure 3, the high MMS scores also verifies that. Another interesting observation is, for causal models GPT, GPT2 and ELMo, they all have higher MMS in their middle layers but lower MMS in the end. This means their initial layer and final layers' embeddings tend to merge. On the contrary, the BERT and DistilBERT have increasing MMS in deeper layers, meaning that the clusters in their embeddings are becoming clearer in deeper layers.

3.4 ISOTROPY IN CENTERED SPACE WITHIN CLUSTERS

As suggest by Mu & Viswanath (2018), the embedding space should be measured after shifting the mean to the origin. We do the mea shifting for each cluster, and calculate the adjusted S'_{inter} . Assuming we have a total of $|C|$ clusters, let $\Phi^c(t) = \{\phi_1^c(t), \phi_2^c(t), \dots\}$ be the set of type t 's embeddings in cluster $c \in C$, and $\phi^c(t)$ be one random sample in $\Phi^c(t)$. Define the adjusted similarity:

$$S'_{\text{inter}} \triangleq \mathbb{E}_c [\mathbb{E}_{i \neq j} [\cos(\bar{\phi}^c(t_i), \bar{\phi}^c(t_j))]] \quad , \quad \text{where} \quad \bar{\phi}^c(t) = \phi^c(t) - \mathbb{E}_{\phi^c} [\phi^c(t)] \quad (3)$$

Here \mathbb{E}_c is the average over different clusters, and $\bar{\phi}^c(t)$ is the original embedding shifted by mean (subtract the mean), where the mean is taken over the samples in cluster c . Similarly we define

$$S'_{\text{intra}} \triangleq \mathbb{E}_c [\mathbb{E}_i [\mathbb{E}_{k \neq l} [\cos(\bar{\phi}_k^c(t_i), \bar{\phi}_l^c(t_i))]]] \quad (4)$$

The Figure 4 illustrates the adjusted cosine similarities S'_{inter} and S'_{intra} . It reveals that:

- For the adjusted inter-type cosine (the left plot), all models are having consistent near-zero S'_{inter} . This means nearly perfect isotropy exists within each cluster, in each layer of all the models. The

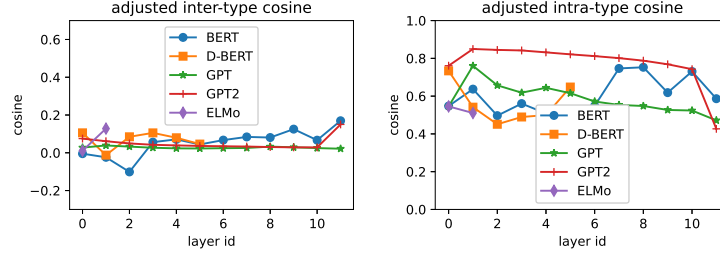


Figure 4: S'_{inter} (left) and S'_{intra} (right). The adjusted S'_{inter} are close to zero, meaning that the space is isotropic under the adjusted measure.

last layer of GPT2 and BERT has slightly worse isotropic behavior, nevertheless, general inter-type isotropy stays across all layers. This reveals the distinguishable embedding vectors.

- The general decreasing trend of intra-type cosine (the right plot) shows that the multiple instances for the same type/word, is slowly spreading over the layers. This is consistent with the un-centered intra-type cosine shown in Figure 1.

4 LOW-DIMENSIONAL MANIFOLDS

4.1 SWISS ROLL MANIFOLD OF GPT/GPT2

While BERT and D-BERT tend to distribute embeddings along more dimensions, GPT and GPT2 embed tokens in low-dimensional manifolds in their contextual embedding spaces. More specifically, we discover that most of the tokens are embedded on a spiral band, and that band gets thicker in the later layers thereafter form a Swiss Roll shaped surface.

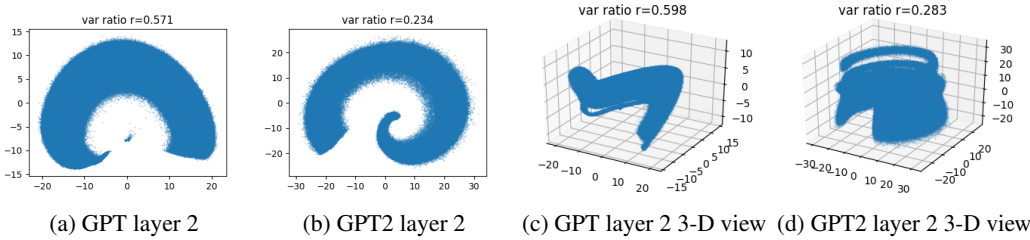


Figure 5: The 2-D and 3-D view of low-dimensional manifold in GPT/GPT2’s embedding spaces

Figure 5a and 5b show the 2-D front view of the manifold in GPT and GPT2. Note that Figure 5a zooms into the large cluster illustrated in Figure 2a (the left one), and discards the smaller one (the right one). 3-D plots are shown in Figure 5c and 5d to demonstrate two manifolds, a band shaped manifold and a Swiss Roll shaped manifold. These plots were computed over PTB dataset. Similar results have been obtained from Wiki2 in supplementary. Figure 6 tracks the progression of a narrow band into a Swiss Roll. The Swiss Roll becomes taller and taller with deeper and deeper layers.

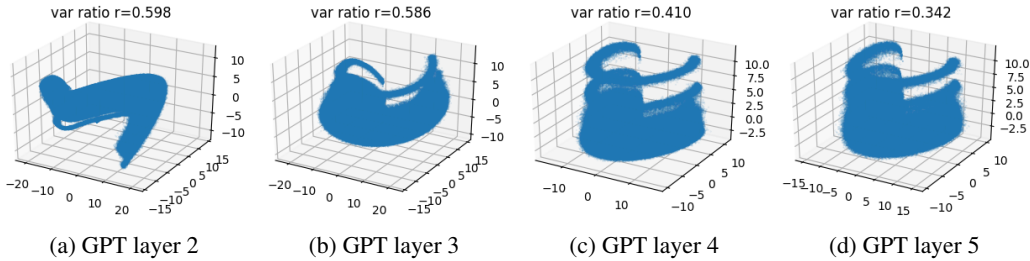
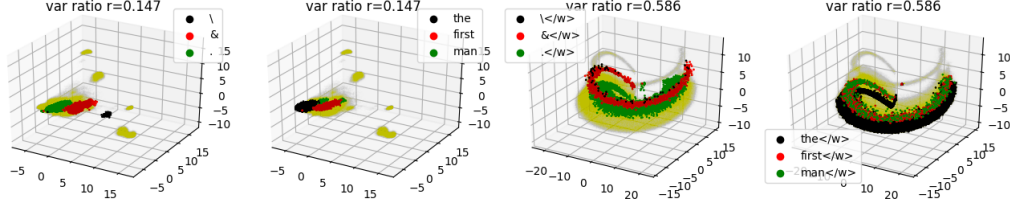


Figure 6: The evolution from a narrow band into a taller and taller Swiss Roll with deeper layers.

4.2 TOKENS IN THE SPACE

To verify the manifold structure in GPT family, we study the token embeddings in the space. It is believed that similar embeddings (e.g. the embeddings for two instances of the same word) tend to stay close together in a Euclidean space, as they should have high cosine similarities. Figure 7 drills down into the embeddings for six frequent words: three punctuation symbols (“\”, “&”, “.”) and three common words (“the”, “first”, “man”). Each panel uses four colors: three colors (black, red, green) for three words of interest, plus gold color for all the other tokens.



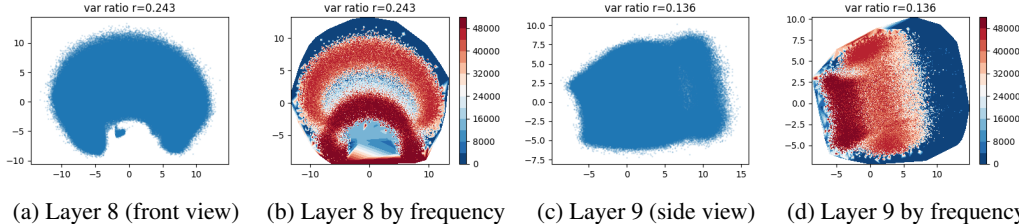
(a) BERT, symbol tokens (b) BERT, word tokens (c) GPT, symbol tokens (d) GPT, word tokens

Figure 7: Embeddings for symbol tokens and word tokens, in layer 3 of BERT and GPT. This shows that GPT has manifold structure, such that vectors are along the spiral band. BERT’s space is closer to a Euclidean space as similar vectors are in concentrated clusters.

As shown in Figure 7a 7b, the BERT model indeed group similar embeddings into small regions in the space (the red, black and green clusters). However, the GPT models are assigning similar embeddings along the manifold we observed before. In Figure 7c 7d, the embeddings for the tokens occupy a spiral band that almost cross the entire space. It does not comply with the Euclidean space geometry as points in such a spiral band would not have high cosine similarity. A Riemannian metric must exist, such that the manifold has larger distance between two spiral bands, but smaller distance on the band. Note that the 3-D plots are obtained using PCA, so there is no density-based nor non-linear reduction involved. Therefore, the manifold structures in GPT embedding spaces are verified.

4.3 WORD FREQUENCY

Another key finding is that all the models are trying to map the high frequent words/types to some specific region in the embedding spaces, rather than spreading them out to the entire space. In Figure 8, embeddings (upper row) and corresponding word frequencies (bottom row) of GPT’s layer 8 and 9 are shown. The darker red denoted higher frequency and blue is lower frequency. The numbers at the colorbar show the number of occurrence (of a particular word / type).



(a) Layer 8 (front view) (b) Layer 8 by frequency (c) Layer 9 (side view) (d) Layer 9 by frequency

Figure 8: Word frequency heatmap in GPT layer 8 and 9. Red is high frequency, blue is low. High frequency words are at the front end of the Swiss Roll, while low frequency words at the other end. (8b 8d are drawn using matplotlib.tricontourf, so the ring at 8b’s bottom should not be closed.)

The Figure 8a 8c are after PCA, and selecting the two most significant dimensions. From GPT layer 8 to layer 9, as the Swiss Roll becomes taller, more variance is accounted for along the height of the Swiss Roll. Thus, the perspective switches from a front view to a side view when moving to layer 9.

Figures 8b and 8d show that the most frequent words appear at the head of the Swiss Roll, followed by bands of less and less frequent words. The least frequent words appear at the far end of the Swiss Roll. This pattern suggests the model distinguishes more frequent from less frequent words. As the model finds more and more rare words, it appends them at the end of the Swiss Roll.

4.4 MANIFOLD LOCAL INTRINSIC DIMENSION

Although the original space dimension is 768 (1024 for ELMo), the manifold we observed has a lower **intrinsic dimension**. It means the data point on the manifold has fewer degrees of freedom to move around. For example, on a Swiss Roll in a 3-D space, any point can only have 2-D freedom thus the intrinsic dimension is only 2. A recent research on the intrinsic dimension for deep networks could be found at (Ansuini et al., 2019). In this section, we adopt the **Local Intrinsic Dimension (LID)** that estimates dimension locally with respect to a reference point. LID is introduced by Houle (2013), and being used in deep learning model characterization recently, e.g. (Ma et al., 2018). The LID is often derived using expansion models (Houle et al., 2012), which tries to obtain the local dimension in the vicinity of a reference point from the growth (expansion) characteristics. To illustrate this, we borrow an example from Ma et al. (2018). Let γ be the radius of an m -D ball in the Euclidean space, denote its volume as ν , then the volume’s growth rate is proportional to γ^m , i.e. $\nu_2/\nu_1 = (\gamma_2/\gamma_1)^m$, from which we can infer the local dimension \tilde{m} by $\tilde{m} = \log(\nu_2/\nu_1) / \log(\gamma_2/\gamma_1)$.

Accurately computing LID is a hard problem which requires a tremendous amount of data samples and enough density around the reference point. So fewer-sample estimate of LID is being studied in the past decade. One of the efficient estimation is proposed by Amsaleg et al. (2015). This technique relies on K nearest neighbor search (K -NN). For a reference point p , denote the set of its K nearest neighbor points as $\Psi_p = \{q_1, \dots, q_K\}$. Then the estimate of LID is computed as: $\tilde{\text{LID}}(p) = -\left(\frac{1}{K} \sum_{i=1}^K \log \frac{\text{dist}(p, q_i)}{\max_i(\text{dist}(p, q_i))}\right)^{-1}$, where the term inside log is the ratio of distance between p to its neighbor, over the maximum distance among them. In our experiments, we use an efficient nearest neighbor computation package FAISS (Johnson et al., 2017) (<https://github.com/facebookresearch/faiss>) to perform the K -NN. We set $K = 100$, the same as in (Aumüller & Ceccarelli, 2019). ℓ_2 distance is used, i.e. $\text{dist}(p, q) = \|p - q\|_2$. We report the mean LID over all the samples as $\mathbb{E}_p[\tilde{\text{LID}}(p)]$, in Figure 9.

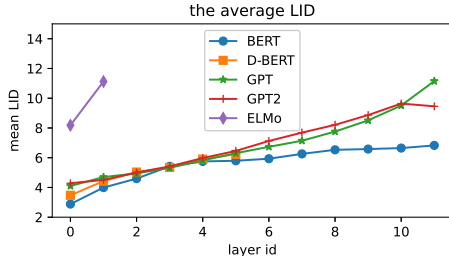


Figure 9: The average LID using Euclidean distance. ELMo’s original embedding dimension is 1024, larger than other models’ 768.

As shown in Figure 9, the mean LIDs for all the models in all the layers are below 12. The small mean LID values reveals that the manifold’s intrinsic dimension is relatively low, especially considering that this is a 768-D (1024 for ELMo) embedding space. Since ELMo’s 1024-D is larger than other models 768-D dimension, its LID is also slightly higher than other models as shown in the figure. In all the contextual embedding layers, there is a clear trend of increasing LID values. In Figure 9, we can also see a nearly-linear relationship between layer id and LID. With deeper and deeper layers in the net, the manifold is diffusing and slowly loses concentration. This would lead to data samples spreading, consistent with Figure 4 (recall that intra-type cosines decrease with depth).

Table 3 compares LIDs for static and contextual embeddings. The table reports results for three static embeddings: GloVe / GloVe-2M (Pennington et al., 2014), and GNEWS (Mikolov et al., 2013a). Results for static embedding LIDs are based on Aumüller & Ceccarelli (2019). Following Aumüller & Ceccarelli (2019), we use cosine distance here: $\text{dist}'(p, q) = 1 - \cos(p, q) = 1 - \frac{\langle p, q \rangle}{\|p\|_2 \|q\|_2}$. Note that estimates for LID using cosines are very close to the estimates using ℓ_2 distances. Table 3 reports averages of LIDs over each model’s layers. Even though GloVe (Pennington et al., 2014) in Table 3 has much fewer embedding dimensions (100-D compared with BERT’s 768-D), the LID is still higher than all of the contextual embedding models. From the table we can find that static embedding spaces generally have higher LID than the contextual ones. This means that the data points are more isotropic in the static embeddings, possibly due to their large vocabularies.

5 CONCLUSIONS AND FUTURE WORK

Previous works have reported the strong anisotropy in deep LMs, which failed to explain the superior performance achieved by these models. We suggest that the anisotropy is a global view being largely misled by distinct clusters resided in the space. Our experiments show that it is more constructive to isolate and transform the space to measure the isotropy. From this view, within the clusters the spaces have almost perfect isotropy that could explain the large model capacity. In addition, we investigate the space geometry for different models. Our visualization demonstrates a low-dimensional Swiss Roll manifold for GPT and GPT2 embeddings, that has not been reported before. The tokens and word frequencies are presented to qualitatively show the manifold structure. We propose to use the approximate LID to quantitatively measure the local subspace, and compared with static embedding spaces. The results show smaller LID values for the contextual embedding models, which can be seen as a local anisotropy in the space. We hope this line of research could bring a comprehensive geometric view of contextual embedding space, and gain insights to further improve the deep LMs’ performance.

Table 3: A comparison of LIDs (using cosine similarity) among contextual and static embedding spaces.

	Model	n	m	avg LID
Contxt Embeds	BERT	1.19 M	768	5.6
	D-BERT	1.19 M	768	7.3
	GPT	0.96 M	768	6.8
	GPT2	1.09 M	768	7.0
	ELMo	0.88 M	1024	9.1
Static Embeds	GloVe	1.18 M	100	18.0
	GloVe-2M	2.20 M	300	26.1
	GNEWS	3.00 M	300	21.1

REFERENCES

- Laurent Amsaleg, Oussama Chelly, Teddy Furon, Stéphane Girard, Michael E Houle, Ken-ichi Kawarabayashi, and Michael Nett. Estimating local intrinsic dimensionality. In *Proceedings of the 21th ACM SIGKDD International Conference on Knowledge Discovery and Data Mining*, pp. 29–38, 2015.
- Alessio Ansuini, Alessandro Laio, Jakob H Macke, and Davide Zoccolan. Intrinsic dimension of data representations in deep neural networks. In *Advances in Neural Information Processing Systems*, pp. 6111–6122, 2019.
- Martin Aumüller and Matteo Ceccarello. The role of local intrinsic dimensionality in benchmarking nearest neighbor search. In *International Conference on Similarity Search and Applications*, pp. 113–127. Springer, 2019.
- David Demeter, Gregory Kimmel, and Doug Downey. Stolen probability: A structural weakness of neural language models. *Proceedings of the 58th Annual Meeting of the Association for Computational Linguistics*, 2020.
- Jacob Devlin, Ming-Wei Chang, Kenton Lee, and Kristina Toutanova. Bert: Pre-training of deep bidirectional transformers for language understanding. *arXiv preprint arXiv:1810.04805*, 2018.
- Martin Ester, Hans-Peter Kriegel, Jörg Sander, Xiaowei Xu, et al. A density-based algorithm for discovering clusters in large spatial databases with noise. In *Kdd*, volume 96, pp. 226–231, 1996.
- Kawin Ethayarajh. How contextual are contextualized word representations? comparing the geometry of bert, elmo, and gpt-2 embeddings. In *Proceedings of the 2019 Conference on Empirical Methods in Natural Language Processing and the 9th International Joint Conference on Natural Language Processing (EMNLP-IJCNLP)*, pp. 55–65, 2019.
- Jun Gao, Di He, Xu Tan, Tao Qin, Liwei Wang, and Tieyan Liu. Representation degeneration problem in training natural language generation models. In *International Conference on Learning Representations*, 2019.
- John Hewitt and Christopher D Manning. A structural probe for finding syntax in word representations. In *Proceedings of the 2019 Conference of the North American Chapter of the Association for Computational Linguistics: Human Language Technologies, Volume 1 (Long and Short Papers)*, pp. 4129–4138, 2019.
- Michael E Houle. Dimensionality, discriminability, density and distance distributions. In *2013 IEEE 13th International Conference on Data Mining Workshops*, pp. 468–473. IEEE, 2013.
- Michael E Houle, Hisashi Kashima, and Michael Nett. Generalized expansion dimension. In *2012 IEEE 12th International Conference on Data Mining Workshops*, pp. 587–594. IEEE, 2012.
- Jeff Johnson, Matthijs Douze, and Hervé Jégou. Billion-scale similarity search with gpus. *arXiv preprint arXiv:1702.08734*, 2017.
- Tianlin Liu, Lyle Ungar, and Joao Sedoc. Unsupervised post-processing of word vectors via conceptor negation. In *Proceedings of the AAAI Conference on Artificial Intelligence*, volume 33, pp. 6778–6785, 2019.
- Xingjun Ma, Bo Li, Yisen Wang, Sarah M Erfani, Sudanthi Wijewickrema, Grant Schoenebeck, Dawn Song, Michael E Houle, and James Bailey. Characterizing adversarial subspaces using local intrinsic dimensionality. In *International Conference on Learning Representations*, 2018.
- Mitchell Marcus, Beatrice Santorini, and Mary Ann Marcinkiewicz. Building a large annotated corpus of english: The penn treebank. 1993.
- Stephen Merity, Caiming Xiong, James Bradbury, and Richard Socher. Pointer sentinel mixture models. *arXiv preprint arXiv:1609.07843*, 2016.
- Tomas Mikolov, Kai Chen, Greg Corrado, and Jeffrey Dean. Efficient estimation of word representations in vector space. *arXiv preprint arXiv:1301.3781*, 2013a.

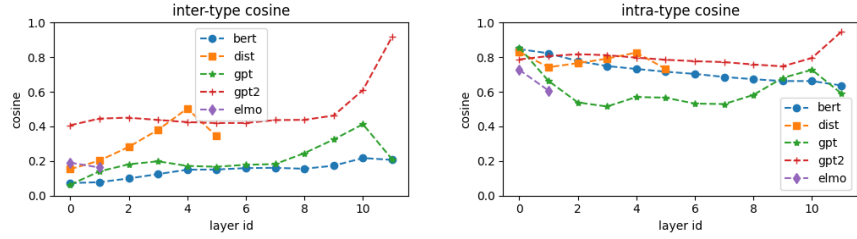
- Tomas Mikolov, Ilya Sutskever, Kai Chen, Greg S Corrado, and Jeff Dean. Distributed representations of words and phrases and their compositionality. In *Advances in neural information processing systems*, pp. 3111–3119, 2013b.
- Jiaqi Mu and Pramod Viswanath. All-but-the-top: Simple and effective post-processing for word representations. In *6th International Conference on Learning Representations, ICLR 2018*, 2018.
- Jeffrey Pennington, Richard Socher, and Christopher D Manning. Glove: Global vectors for word representation. In *Proceedings of the 2014 conference on empirical methods in natural language processing (EMNLP)*, pp. 1532–1543, 2014.
- Matthew E Peters, Mark Neumann, Mohit Iyyer, Matt Gardner, Christopher Clark, Kenton Lee, and Luke Zettlemoyer. Deep contextualized word representations. *arXiv preprint arXiv:1802.05365*, 2018.
- Steven T. Piantadosi. Zipf’s word frequency law in natural language: A critical review and future directions. *Psychonomic bulletin & review*, 21(5):1112–1130, 2014.
- Alec Radford, Karthik Narasimhan, Tim Salimans, and Ilya Sutskever. Improving language understanding by generative pre-training, 2018.
- Alec Radford, Jeffrey Wu, Rewon Child, David Luan, Dario Amodei, and Ilya Sutskever. Language models are unsupervised multitask learners. *OpenAI Blog*, 1(8):9, 2019.
- Emily Reif, Ann Yuan, Martin Wattenberg, Fernanda B Viegas, Andy Coenen, Adam Pearce, and Been Kim. Visualizing and measuring the geometry of bert. In *Advances in Neural Information Processing Systems*, pp. 8594–8603, 2019.
- Peter J Rousseeuw. Silhouettes: a graphical aid to the interpretation and validation of cluster analysis. *Journal of computational and applied mathematics*, 20:53–65, 1987.
- Victor Sanh, Lysandre Debut, Julien Chaumond, and Thomas Wolf. Distilbert, a distilled version of bert: smaller, faster, cheaper and lighter. *arXiv preprint arXiv:1910.01108*, 2019.
- Yu Sun, Shuohuan Wang, Yukun Li, Shikun Feng, Xuyi Chen, Han Zhang, Xin Tian, Danxiang Zhu, Hao Tian, and Hua Wu. Ernie: Enhanced representation through knowledge integration. *arXiv preprint arXiv:1904.09223*, 2019.

SUPPLEMENTARY: FULL RESULTS ON PTB AND WIKI2 DATASETS

A RESULTS ON WIKI2 DATASET

A.1 THE UNADJUSTED INTER AND INTRA COSINE SIMILARITY

Note that "dist" in the following legends represents DistilBERT model.

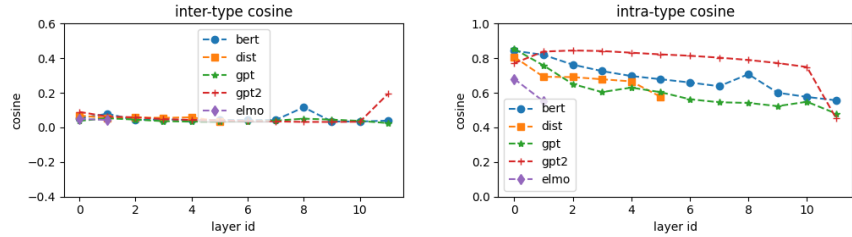


(a) Inter-type cosine similarity. As layers goes deeper, inter-type cosine goes higher. All models' last layer behaves slightly differently.

(b) Intra-type cosine similarity. The intra-type cosine decreases showing the same type's embedding instances are spreading in deeper layers.

A.2 THE CENTER-SHIFTED AND CLUSTERED COSINE SIMILARITY

The inter-type and intra-type cosines are adjusted using the proposed center-shifting and clustering methods. Now it reflects the isotropicity in almost all layers in all models.



(a) The clustered inter-type cosine (center shifted). It shows strong isotropicity as the average cosine between different types is close to 0 across all layers in all models. The GPT2's last layer still has slightly higher cosine compared with others.

(b) The clustered intra-type cosine (center shifted). The intra-type cosines are much more consistent than the unadjusted counterpart (the cosine decreases nearly monotonically as layers goes deeper).

A.3 THE APPROXIMATE LOCAL INTRINSIC DIMENSIONS

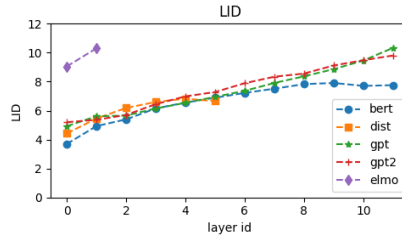
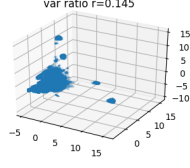


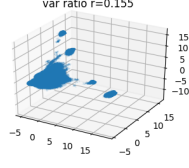
Figure 12: Local Intrinsic Dimensions. The LID increases as layer goes deeper, reflecting embeddings spreading out in all models' deeper layers (becoming more locally isotropic).

B FULL VISUALIZATION - PTB DATASET

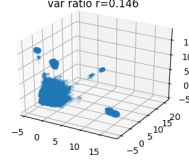
B.1 BERT



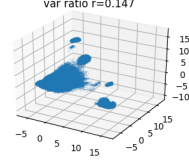
(a) BERT layer 0



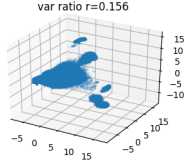
(b) BERT layer 1



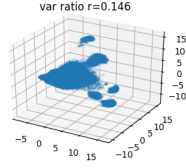
(c) BERT layer 2



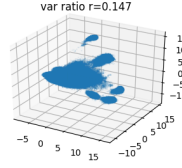
(d) BERT layer 3



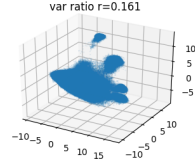
(e) BERT layer 4



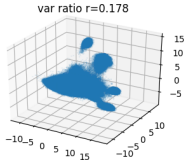
(f) BERT layer 5



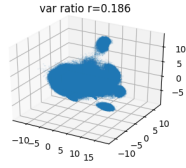
(g) BERT layer 6



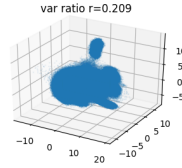
(h) BERT layer 7



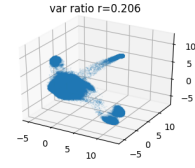
(i) BERT layer 8



(j) BERT layer 9

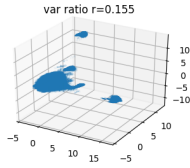


(k) BERT layer 10

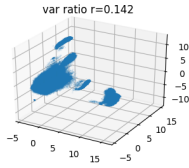


(l) BERT layer 11

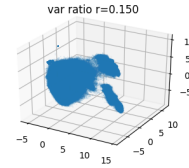
B.2 DISTILBERT AND ELMo



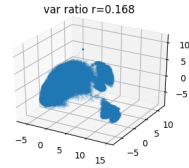
(a) DistilBERT layer 0



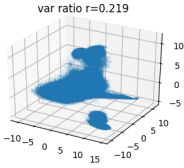
(b) DistilBERT layer 1



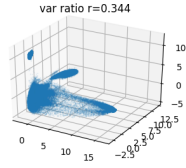
(c) DistilBERT layer 2



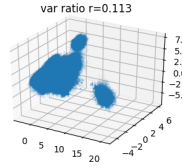
(d) DistilBERT layer 3



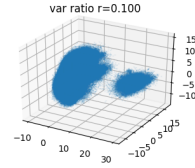
(e) DistilBERT layer 4



(f) DistilBERT layer 5

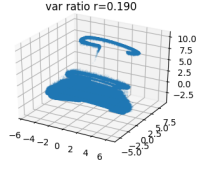


(g) ELMo layer 0

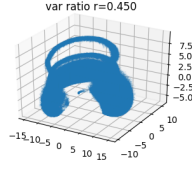


(h) ELMo layer 1

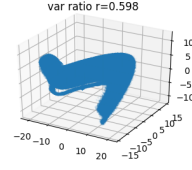
B.3 GPT



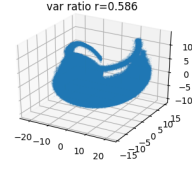
(a) GPT layer 0



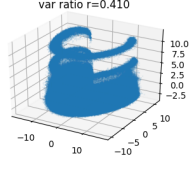
(b) GPT layer 1



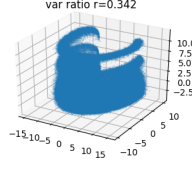
(c) GPT layer 2



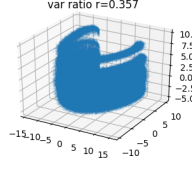
(d) GPT layer 3



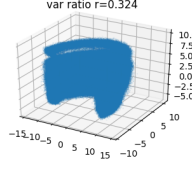
(e) GPT layer 4



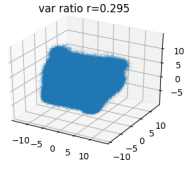
(f) GPT layer 5



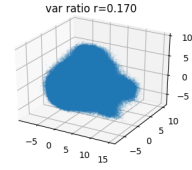
(g) GPT layer 6



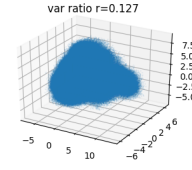
(h) GPT layer 7



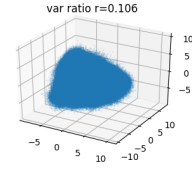
(i) GPT layer 8



(j) GPT layer 9

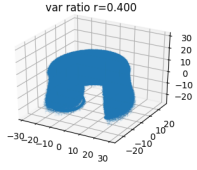


(k) GPT layer 10

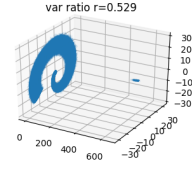


(l) GPT layer 11

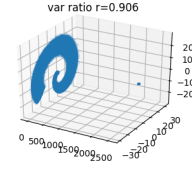
B.4 GPT2



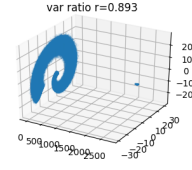
(a) GPT2 layer 0



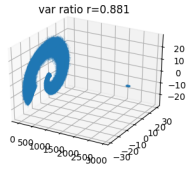
(b) GPT2 layer 1



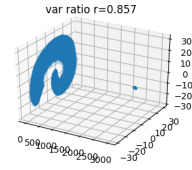
(c) GPT2 layer 2



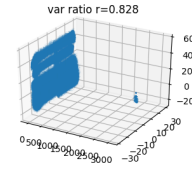
(d) GPT2 layer 3



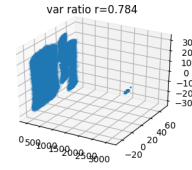
(e) GPT2 layer 4



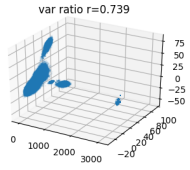
(f) GPT2 layer 5



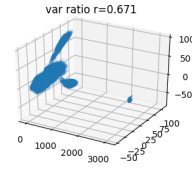
(g) GPT2 layer 6



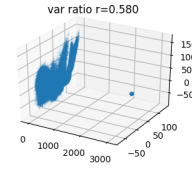
(h) GPT2 layer 7



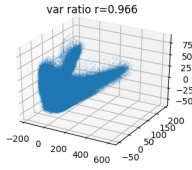
(i) GPT2 layer 8



(j) GPT2 layer 9



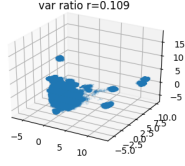
(k) GPT2 layer 10



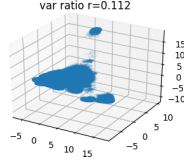
(l) GPT2 layer 11

C FULL VISUALIZATION - WIKI2 DATASET

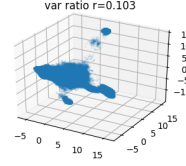
C.1 BERT



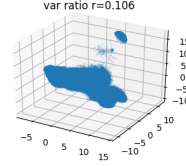
(a) BERT layer 0



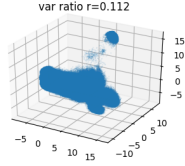
(b) BERT layer 1



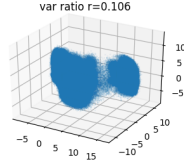
(c) BERT layer 2



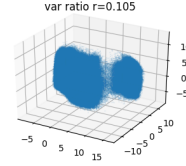
(d) BERT layer 3



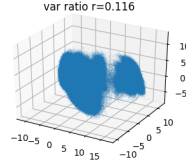
(e) BERT layer 4



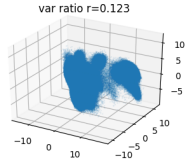
(f) BERT layer 5



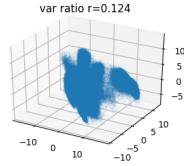
(g) BERT layer 6



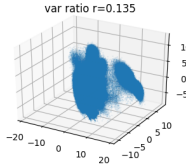
(h) BERT layer 7



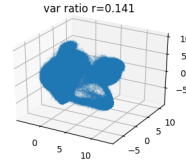
(i) BERT layer 8



(j) BERT layer 9

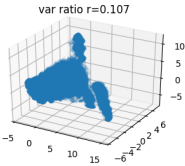


(k) BERT layer 10

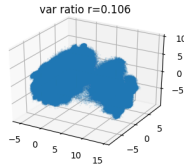


(l) BERT layer 11

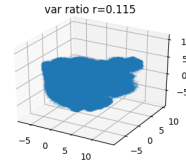
C.2 DISTILBERT



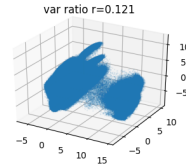
(a) DistilBERT layer 0



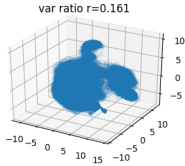
(b) DistilBERT layer 1



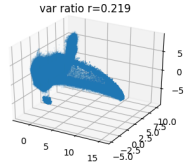
(c) DistilBERT layer 2



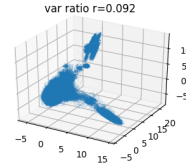
(d) DistilBERT layer 3



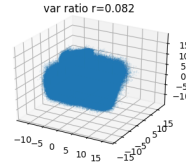
(e) DistilBERT layer 4



(f) DistilBERT layer 5

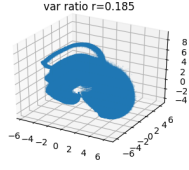


(g) ELMo layer 0

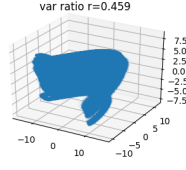


(h) ELMo layer 1

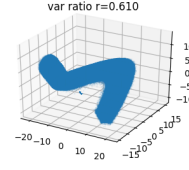
C.3 GPT



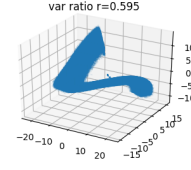
(a) GPT layer 0



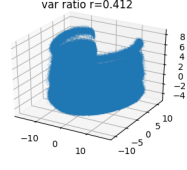
(b) GPT layer 1



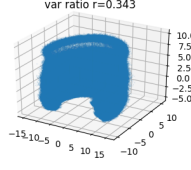
(c) GPT layer 2



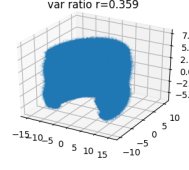
(d) GPT layer 3



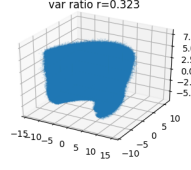
(e) GPT layer 4



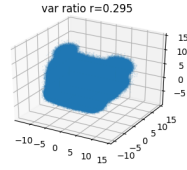
(f) GPT layer 5



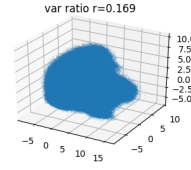
(g) GPT layer 6



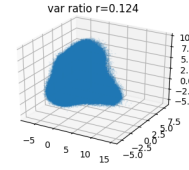
(h) GPT layer 7



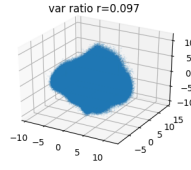
(i) GPT layer 8



(j) GPT layer 9

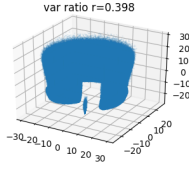


(k) GPT layer 10

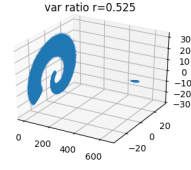


(l) GPT layer 11

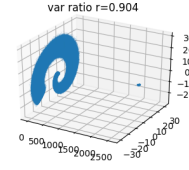
C.4 GPT2



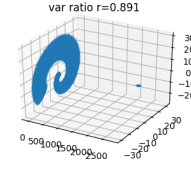
(a) GPT2 layer 0



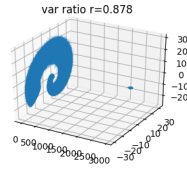
(b) GPT2 layer 1



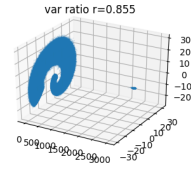
(c) GPT2 layer 2



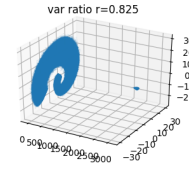
(d) GPT2 layer 3



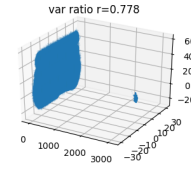
(e) GPT2 layer 4



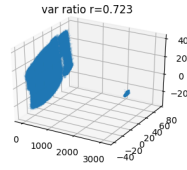
(f) GPT2 layer 5



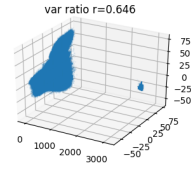
(g) GPT2 layer 6



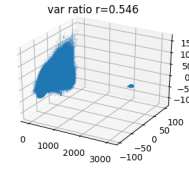
(h) GPT2 layer 7



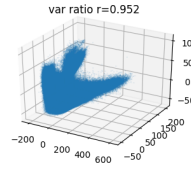
(i) GPT2 layer 8



(j) GPT2 layer 9



(k) GPT2 layer 10



(l) GPT2 layer 11